

# Road Surface Roughness Assessment: A Spaceborne SAR-Based Approach

Arun Babu<sup>a</sup>, Dominik Gerber<sup>a</sup>, Stefan V. Baumgartner<sup>a</sup>, Gerhard Krieger<sup>a</sup>,  
<sup>a</sup>Microwaves and Radar Institute, German Aerospace Center (DLR), Wessling, Germany  
Email: Arun.Babu@dlr.de

## Abstract

Road surface roughness has a strong influence on vehicle skid resistance and road safety, requiring periodic assessment to perform maintenance activities. This study introduces a novel method for large-scale road surface roughness estimation using high-resolution X-band SAR data from Germany's TerraSAR-X satellite. The method accommodates spaceborne SAR's low SNR by utilizing techniques like multilooking, SNR thresholding, and multi-dataset fusion. Techniques like geocoding and automated road extraction are incorporated to enhance the interpretability of the results. The road surface roughness values estimated through this method aligns closely with ground truth data and also with results obtained using DLR's airborne F-SAR system.

## 1 Introduction

The role of safe road infrastructure is indispensable in a nation's progress, as it establishes a dependable transportation network for people, goods, and services. One of the critical factors of road safety is the quality of the road surface itself. For example, the road surface roughness directly influences the friction between the road and vehicle tires [1]. Adequate friction is essential for safe acceleration, braking, and steering, while insufficient friction can lead to accidents [2]. Conversely, excessive friction may result in passenger discomfort and increased fuel usage. Therefore, the regular assessment of road surface roughness is important to maintain it within the optimal limits [3]. Presently, specialized survey vehicles are employed to assess road quality, measuring parameters like road friction and unevenness. However, conducting such surveys across an entire country can be time-intensive, laborious, and therefore costly. Consequently, these assessments are conducted infrequently, often with intervals of several years, such as the four-year cycle employed in Germany [4]. The sensitivity of synthetic aperture radar (SAR) to variations in surface roughness positions it as a promising tool for assessing road surface roughness over large areas. Airborne SAR systems offer the capability to capture fully polarimetric, high-resolution data in stripmap mode, delivering a high signal-to-noise ratio (SNR) and good swath coverage. Previous studies have been successfully conducted by the German Aerospace Center (DLR) to produce road surface roughness images using high-resolution fully polarimetric airborne X-band SAR datasets acquired by the F-SAR system [3], [5]. However, airborne SAR systems are constrained by their high operational costs, the necessity for precise flight planning, and limited coverage. In contrast, state-of-the-art spaceborne SAR systems in general need to be operated in spotlight mode for achieving a comparably high spatial resolution, but this generally confines them to a smaller scene size per acquisition. Additionally, their SNR is reduced due to increased sensor alti-

tude. Nevertheless, spaceborne SAR systems offer the distinct advantage of global data acquisition at a reduced cost [6]. Within the scope of this study, a semi-empirical model has been developed to estimate the road surface roughness using high-resolution X-band spaceborne SAR datasets acquired by Germany's TerraSAR-X (TS-X) satellite.

## 2 Study areas and Datasets

To conduct this study, it is necessary to select areas with surfaces constructed using typical road-building materials having varying surface roughness values such as concrete, asphalt, or comparable materials. Accordingly, two such study areas were identified.

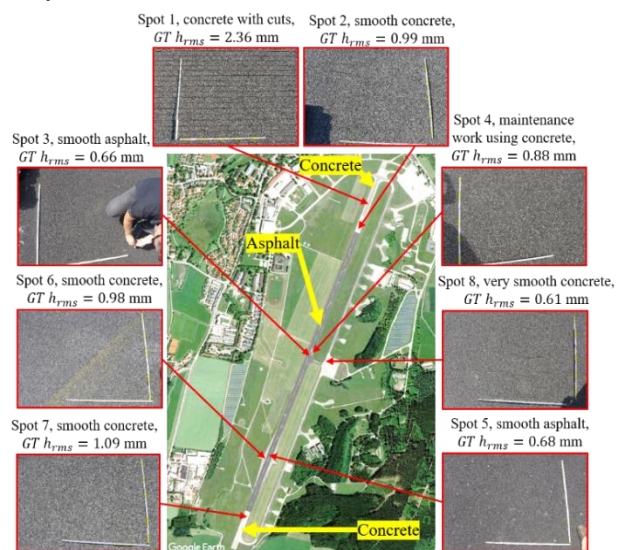


Figure 1 Kaufbeuren study area.

The first study area is the Kaufbeuren airfield located in Bavaria, which is a former military airfield comprising runways, taxiways, and parking areas that are no longer in use. The runway ends are constructed of concrete, while the

middle portion is made of asphalt (cf. **Figure 1**). A ground truth (GT) data collection activity was conducted here to train the road surface roughness estimation models and to validate the results. For this purpose, eight GT spots with a 1 m<sup>2</sup> area were selected on the runway and taxiway, which were smooth, rough, and made of different materials such as asphalt and concrete, thereby providing varying levels of surface roughness. The locations and photos of each of these GT spots are shown in **Figure 1**. The surface undulation values of each GT spot were measured using a handheld laser scanner with micrometer accuracy. Since the root mean square height ( $h_{\text{rms}}$ ) is commonly used as a measure of vertical surface roughness, the surface undulation values obtained for each GT spots were utilized to calculate a single GT road surface roughness value (GT  $h_{\text{rms}}$ ) for each GT spot using the following equation [7]:

$$h_{\text{rms}} = \sqrt{\frac{\sum_{i=1}^n (h_i - \bar{h})^2}{n - 1}}, \quad (1)$$

where  $h_i$  is the surface undulation value measured for the  $i^{\text{th}}$  sample,  $\bar{h}$  is the mean of all the surface undulation values and  $n$  is the number of surface undulation values. The GT  $h_{\text{rms}}$  values computed for each of the GT spots are provided in **Figure 1**.



**Figure 2** Wolfsburg motorway crossing, Braunschweig.

The second study area is the Wolfsburg motorway crossing in Braunschweig. This area comprises long motorways (cf. **Figure 2**) where consistent surface roughness is anticipated. Nevertheless, there may be sudden shifts in road surface roughness values in certain areas, possibly due to the use of materials with varying surface roughness during maintenance activities. For instance, in the section of the motorway depicted in the zoomed-in view, a noticeable shift in the appearance of the road surface is evident, indicating a sudden variation in road surface roughness.

**Table 1** Metadata of the TS-X datasets used.

| Study area   | Date       | Pol | Incidence angle (°) | Use   |
|--------------|------------|-----|---------------------|-------|
| Kaufbeuren   | 16.03.2014 | HH  | 43.7                | Train |
| Kaufbeuren   | 13.08.2022 | VV  | 31.6                | Train |
| Kaufbeuren   | 23.09.2022 | VV  | 43.7                | Train |
| Kaufbeuren   | 29.09.2022 | VV  | 31.0                | Train |
| Braunschweig | 14.02.2023 | VV  | 26.5                | Test  |
| Braunschweig | 21.02.2023 | VV  | 25.5                | Test  |

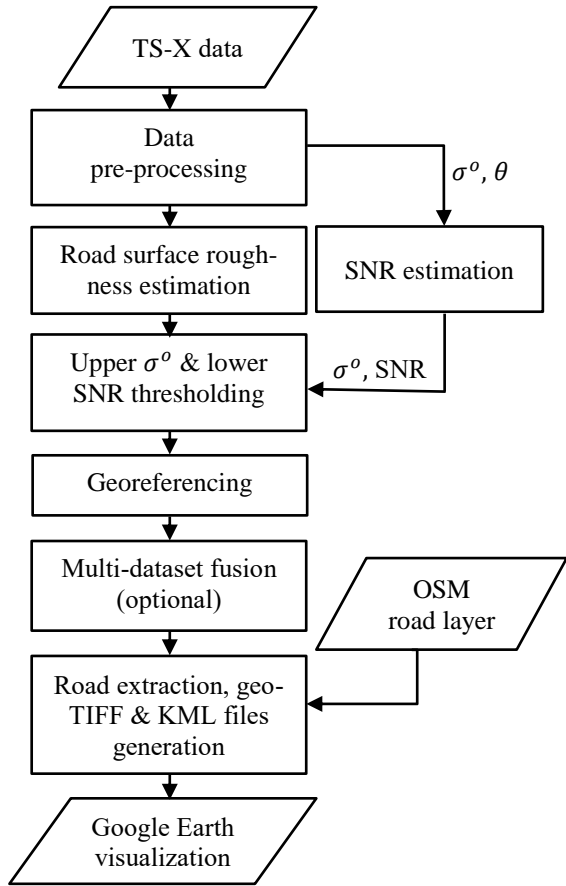


**Figure 3** Block diagram of the processing chain.

This study utilized six TS-X datasets acquired in staring spotlight (ST) mode, offering an approximate spatial resolution of 0.24 x 0.60 m (azimuth x range) and covering a swath area of 3.7 x 4 km (azimuth x range) [8]. The metadata of these datasets can be found in **Table 1**.

### 3 Methodology

To prepare the TS-X datasets for analysis, pre-processing is essential to create noise-minimized sigma nought ( $\sigma^0$ ) backscatter images. These noise-minimized  $\sigma^0$  images serve as a valuable tool for comparing backscatter measurements across different surfaces and allow for the estimation of surface properties, including roughness [6]. Consequently, a  $\sigma^0$  image, in conjunction with the local incidence angle ( $\theta$ ), serves as the input data for the semi-empirical road surface roughness model. **Figure 3** illustrates the block diagram of the processing chain utilized to generate the surface roughness images from the TS-X datasets.

#### 3.1 Pre-processing of the spaceborne SAR data

The pre-processing of the TS-X datasets acquired in ST mode begins with the estimation of  $\sigma^0$  values for each pixel, without employing any spatial averaging. Additionally, noise-equivalent beta nought (NEBN) values are estimated and subtracted from the  $\sigma^0$  values to effectively minimize additive noise [9]. Following this noise reduction

step, multilooking is applied in the spatial domain to mitigate speckle and enhance the SNR. This is achieved by averaging neighboring pixels both in the range and azimuth directions. The size of the sliding window for spatial averaging is determined based on the smallest multilooking factors required in both azimuth and range directions to create approximately square pixels, facilitating easier interpretation of the resulting images.

### 3.2 Road surface roughness estimation

The SAR data can be used to estimate the effective vertical surface roughness ( $ks$ ) parameter, which can be inverted to calculate the  $h_{\text{rms}}$  using the following equation [7]:

$$h_{\text{rms}} = \frac{ks}{(2\pi/\lambda_c)}, \quad (2)$$

where  $\lambda_c$  is the wavelength of the SAR system.

The SAR polarimetry-based methods, SAR backscatter-based semi-empirical models, and physical models that currently exist for estimating roughness ( $ks$  parameter) were initially developed for agricultural fields. However, the previous study showed that these methods cannot be applied to road surfaces due to the significant differences in their properties [3]. Therefore, a new semi-empirical surface roughness model based on the assumptions from the Dubois model [10] was developed in this previous study to reliably estimate road surface roughness using DLR's airborne X-band F-SAR system. The following equation can be used to estimate the  $ks$  parameter using this model [3]:

$$ks = 10^{\left[ \frac{\log(\sigma_{\text{pq}}^o) - \log(\delta(\cos(\theta))^\beta)}{\varepsilon \sin(\theta)} \right]} \quad (3)$$

where,  $\sigma_{\text{pq}}^o$  represents the sigma nought values for the  $p$  transmitted and  $q$  received polarizations, while  $\theta$  denotes the incidence angle. Additionally,  $\delta$ ,  $\beta$ , and  $\varepsilon$  represent the model coefficients. This model has a validity range of  $\theta > 30^\circ$  and  $ks < 2.5$  (which corresponds to  $h_{\text{rms}} < 12.43$  mm for X-band). This model was adapted in this study to estimate road surface roughness using the TS-X datasets. Compared to the F-SAR datasets, the TS-X datasets used in this study are single-polarized, were acquired in ST mode, have coarser resolution, and have lower SNR. Therefore, new model coefficients are estimated to make the model suitable for the TS-X data. The process of estimating these model coefficients involves separate calculations for the HH and VV polarizations. This estimation is performed by a least squares-based curve fitting algorithm. The input data for this coefficient estimation includes the GT  $h_{\text{rms}}$  values,  $\sigma^o$  values, and local incidence angle ( $\theta$ ) values at the ground truth locations. The new set of model coefficients estimated for the TS-X datasets are shown in **Table 2**. For more detailed information on the development of this model refer to [3], [6].

**Table 2** Model coefficients estimated for the TS-X data.

| Coefficients  | Polarization |             |
|---------------|--------------|-------------|
|               | HH           | VV          |
| $\delta$      | 0.16373946   | 0.17887929  |
| $\beta$       | -0.10682052  | -3.95021343 |
| $\varepsilon$ | 1.99490104   | 3.38223192  |

### 3.3 Post-processing of the results

Errors in estimating road surface roughness can occur due to high  $\sigma^o$  values that do not correspond to the actual road surface. This can be caused by strong backscattering from objects like lane dividers, overhead signboards, flyovers, and bridge walls, leading to invalid high surface roughness values. To address this, pixels with  $\sigma^o$  greater than -10 dB were excluded from the final surface roughness ( $h_{\text{rms}}$ ) image generated using the TS-X datasets. Additionally, very low SNR pixels can result in unreliable surface roughness estimates due to noise dominance. To mitigate this, surface roughness values from areas with an SNR below specified a threshold should be excluded. The minimum required SNR threshold for the adapted semi-empirical model to reliably estimate the  $h_{\text{rms}}$  values is 2.5 dB and all pixels having an SNR below this threshold were removed from the final  $h_{\text{rms}}$  image. Both the upper  $\sigma^o$  and lower SNR thresholds were estimated experimentally from the TS-X data used in this study and more details can be found in [6].

Each SAR dataset has a specific acquisition geometry and the  $h_{\text{rms}}$  values estimated using single SAR datasets can be unreliable at some regions having shallow incidence angles, speckle, or very low SNR. This can be addressed by fusing  $h_{\text{rms}}$  images from multiple SAR datasets with different incidence angles and acquisition geometries into a single  $h_{\text{rms}}$  image. The first fusion method, based on the highest SNR, selects  $h_{\text{rms}}$  values on a pixel-wise basis from SAR datasets with the lowest noise. It identifies the pixels with the highest SNR across all datasets, highlighting fine road details but it is potentially sensitive to local backscatter variations. The second method, known as multi-dataset averaging, treats all  $h_{\text{rms}}$  values as reliable. It generates the final  $h_{\text{rms}}$  image by averaging  $h_{\text{rms}}$  values from all datasets, resulting in a smoother image that may lose some smaller road details [3], [6].

Finally, to display the  $h_{\text{rms}}$  images on Google Earth (GE), the images were geocoded from the slant-range coordinate system to a geographic coordinate system. Using the Open Street Map (OSM) road layer, the roads were extracted from the  $h_{\text{rms}}$  images. KML files were then generated to display the road surface roughness images in GE [3], [6].

## 4 Experimental results

The road surface roughness results obtained experimentally are discussed here.

**Figure 4** shows SNR plots created for the runway in the Kaufbeuren study area, representing SNR values at 40 randomly selected positions along the entire length of the runway. These plots include datasets with different incidence angles and polarizations. From **Figure 4**, it can be seen that the concrete surface has a higher SNR compared to the asphalt surface. This observation indicates that the concrete surface has a rougher texture and leads to a stronger backscatter signal. The HH polarization dataset has the lowest SNR, especially in the asphalt regions, making it unsuitable for accurate roughness estimation. In contrast, the VV polarization data exhibit much higher SNR, with

the VV dataset having the highest SNR among the selected datasets at an incidence angle of  $31.6^\circ$ . Therefore, for road surface roughness estimation, TS-X VV polarization datasets with incidence angles between 30 and 35 degrees are the preferred choice, as they ensure an SNR of at least 2.5 dB in both concrete and asphalt areas. Importantly, this selection is also consistent with the validity conditions of the roughness estimation model, which starts at incidence angles of 30 degrees and above.

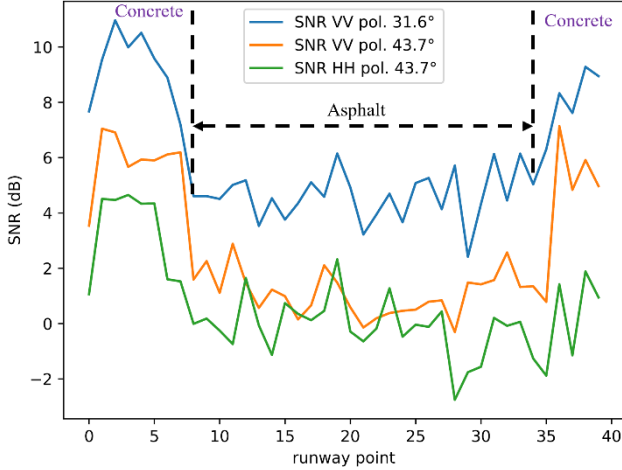


**Figure 4** SNR plot for the Kaufbeuren runway.

In **Figure 5**,  $h_{\text{rms}}$  images of a segment of the Kaufbeuren runway are presented. Following road extraction and KML file creation, these images were superimposed onto GE. The GE image (**Figure 5(a)**) showcases the runway with distinct sections of asphalt, smooth concrete, and rough concrete with repeated cuts. The  $h_{\text{rms}}$  image in **Figure 5(b)** is derived from the F-SAR dataset with a resolution of 25 cm. Comparing this image with **Figure 5(a)**, it can be seen that asphalt areas are depicted in blue, signifying low  $h_{\text{rms}}$  values, while smooth concrete areas appear rougher and are denoted by cyan. Concrete sections with repeated cuts exhibit the highest level of roughness, depicted in yellow. **Figure 5(c)** displays the  $h_{\text{rms}}$  image generated using the TS-X HH polarization dataset. A majority of pixels from asphalt and smooth concrete areas are masked out due to an SNR lower than the 2.5 dB threshold. In **Figure 5(d)**, the  $h_{\text{rms}}$  image is estimated using the TS-X VV polarization dataset. **Figure 5(d)** contains more valid pixels compared to **Figure 5(c)** due to the higher SNR provided by the VV polarization dataset. Asphalt areas are indicated by blue, while smooth concrete areas appear rougher in cyan. The concrete areas with cuts have the highest roughness level, represented by yellow with a value of approximately 2.25 mm. These findings align with the  $h_{\text{rms}}$  results from the F-SAR dataset in **Figure 5(b)**. **Figures 5(e)** and **(f)** illustrate the  $h_{\text{rms}}$  images obtained by fusing multiple datasets using the highest SNR method and the multi-dataset averaging method, respectively. This fusion incorporates all three VV-polarized TS-X datasets available for the Kaufbeuren study area listed in **Table 1**. In both images, asphalt areas are represented in blue to cyan colors, and smooth concrete areas appear entirely in cyan. **Figure 5(e)** exhibits more yellow pixels in the concrete area with cuts

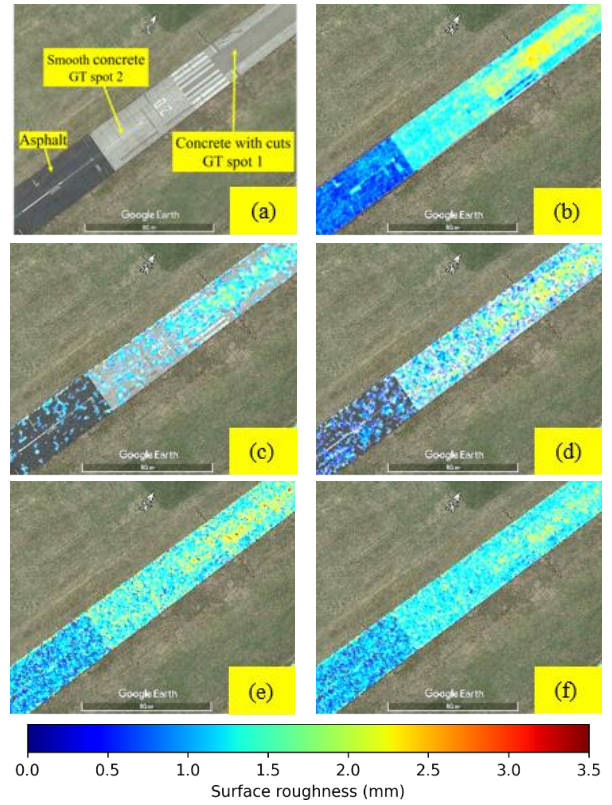
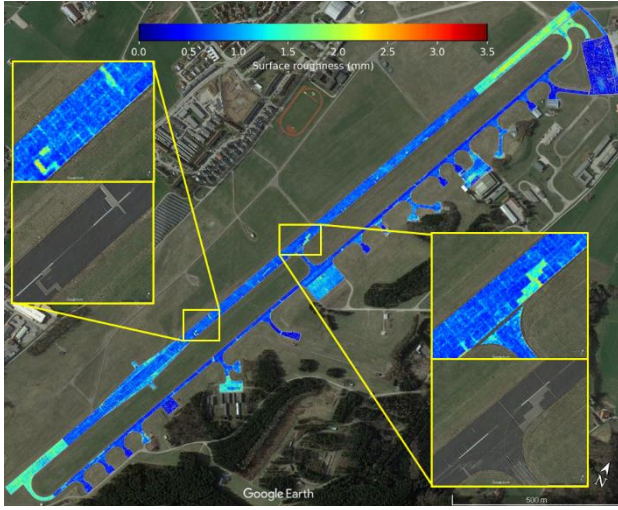


**Figure 5** Depictions of the Kaufbeuren runway featuring (a) a GE image, and (b)  $h_{\text{rms}}$  images derived from (b) F-SAR, (c) TS-X HH polarization, and (d) TS-X VV polarization. Additionally, multi-dataset fusion results are displayed using both the (e) highest SNR method and (f) multi-dataset averaging method.

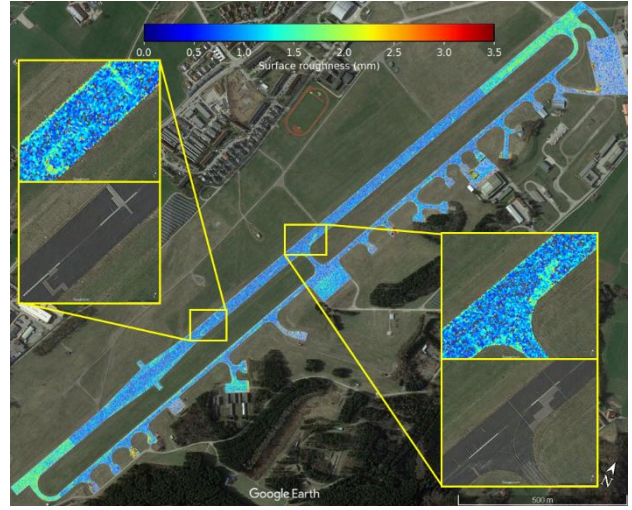
compared to **Figure 5(f)**, indicating a higher level of surface roughness. In both cases, the results closely align with the F-SAR results.

The fused  $h_{\text{rms}}$  images for the entire Kaufbeuren study area, generated using the multi-dataset averaging method, are presented in **Figure 6**. **Figure 6(a)** displays the  $h_{\text{rms}}$  image resulting from the F-SAR datasets, while **(b)** showcases the  $h_{\text{rms}}$  image obtained from the TS-X datasets. In both of these images, it is evident that the concrete regions situated at either end of the runway exhibit a higher degree of roughness compared to the asphalt regions in between, as previously discussed in **Figure 5**. Furthermore, these images reveal the repair work conducted on the runway, particularly in the zoomed views, where these regions exhibit noticeably higher surface roughness, likely due to the use of materials with different compositions during maintenance activities. Notably, the very small cuts on the runway are noticeable exclusively in **Figure 6(a)**, attributable to the very high spatial resolution of the F-SAR datasets (25 cm). Despite the relatively fewer valid pixels in **Figure 6(b)**, a consequence of the lower SNR of the TS-X datasets in comparison to **Figure 6(a)**, the  $h_{\text{rms}}$  values estimated using both the F-SAR and TS-X datasets fall within the similar range and exhibit consistency between them.

**Figure 7** presents a comprehensive analysis of  $h_{\text{rms}}$  plots derived from both TS-X and F-SAR datasets in comparison with the GT  $h_{\text{rms}}$  data. The GT  $h_{\text{rms}}$  values for the eight GT



(a)



(b)

**Figure 6** Fused  $h_{\text{rms}}$  images for the Kaufbeuren study area generated using the multi-dataset averaging method from (a) F-SAR and (b) TS-X datasets.

spots are illustrated by the black plot, while the blue plot represents the  $h_{\text{rms}}$  values estimated from the F-SAR dataset. Although the blue plot generally aligns with the GT  $h_{\text{rms}}$  plot, over- and underestimations are observable for certain GT spots. Overall, these plots exhibit a root mean square error (RMSE) of 0.30 mm. The green plot showcases  $h_{\text{rms}}$  values estimated using the VV-polarized TS-X dataset, featuring an incidence angle of 31.6 degrees. This green plot closely matches the GT  $h_{\text{rms}}$  plot, with an RMSE of 0.32 mm. It is important to note that this dataset was employed for calculating the model coefficients, and the F-SAR  $h_{\text{rms}}$  image, which exhibits an RMSE of 0.30 mm, was utilized as supplementary reference data. Consequently, the RMSE of the TS-X roughness data cannot be less than 0.30 mm. In contrast, the orange plot, generated through multi-dataset fusion using the highest SNR method, tends to overestimate the  $h_{\text{rms}}$  values, yielding the highest RMSE of 0.51 mm. This discrepancy is possibly attributed to its sensitivity to local backscatter variations. The purple plot, resulting from the multi-dataset averaging fusion method, demonstrates an RMSE of 0.42 mm when compared to the GT  $h_{\text{rms}}$  plot. In summary, **Figure 7** offers

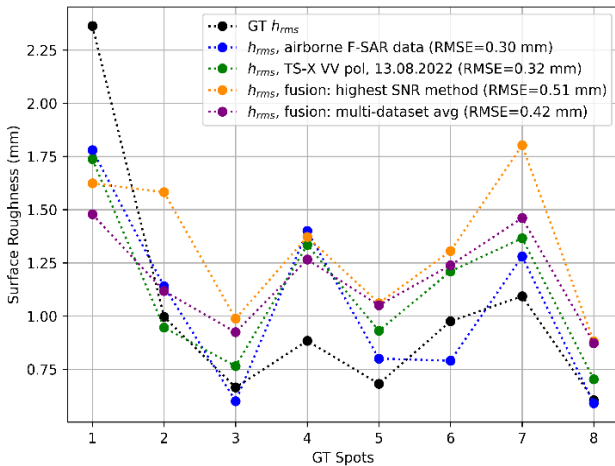


**Figure 7** Comparison of  $h_{\text{rms}}$  plots from TS-X and F-SAR datasets with GT  $h_{\text{rms}}$  plot.

valuable insights, indicating that the TS-X VV-polarized datasets can provide reliable  $h_{\text{rms}}$  estimations, exhibiting a comparable RMSE to both the F-SAR and GT data.

**Figure 8** presents a comparative analysis of the  $h_{\text{rms}}$  images generated for the Wolfsburg motorway crossing, utilizing both the F-SAR and TS-X datasets. Specifically, **Figure 8(a)** displays the  $h_{\text{rms}}$  image derived from a single F-SAR dataset, while **Figure 8(b)** showcases the fused  $h_{\text{rms}}$  image generated through the multi-dataset averaging method, utilizing the two VV-polarized TS-X datasets listed in **Table 1**. In both of these images, the motorway in the east-west direction predominantly appears in blue, indicating a consistent road surface roughness. However, towards the eastern end of the motorway, a sudden transition to cyan becomes evident, signifying an abrupt change in road surface roughness. This could be due to the use of materials with differing compositions during road construction or maintenance activities in this particular area. This change in appearance aligns with the observations in the GE image displayed in **Figure 2**, providing further support for this explanation. A noteworthy observation is the close agreement between the F-SAR and TS-X  $h_{\text{rms}}$  results for this east-west motorway. Conversely, the  $h_{\text{rms}}$  results derived from the TS-X datasets for the north-south motorway exhibit greater noise compared to the F-SAR result. This noise arises because the north-south direction aligns with the azimuth direction of the satellite in the sun-synchronous dusk-dawn orbit, with a  $97^\circ$  inclination. Moving vehicles in the azimuth direction of the SAR system create disturbances in the SAR image. In contrast, the  $h_{\text{rms}}$  result obtained using the F-SAR dataset remains consistently smooth for the north-south motorway and matches the surface roughness values observed for the east-west motorway (blue color). This is because the north-south motorway is not within the azimuth/flight direction of the F-SAR system during data acquisition, as indicated by the azimuth and range direction arrows in **Figure 8(a)**. Therefore, to obtain reliable surface roughness estimates for north-south-oriented roads using the TS-X satellite, data acquisition should ideally occur during periods of reduced traffic.

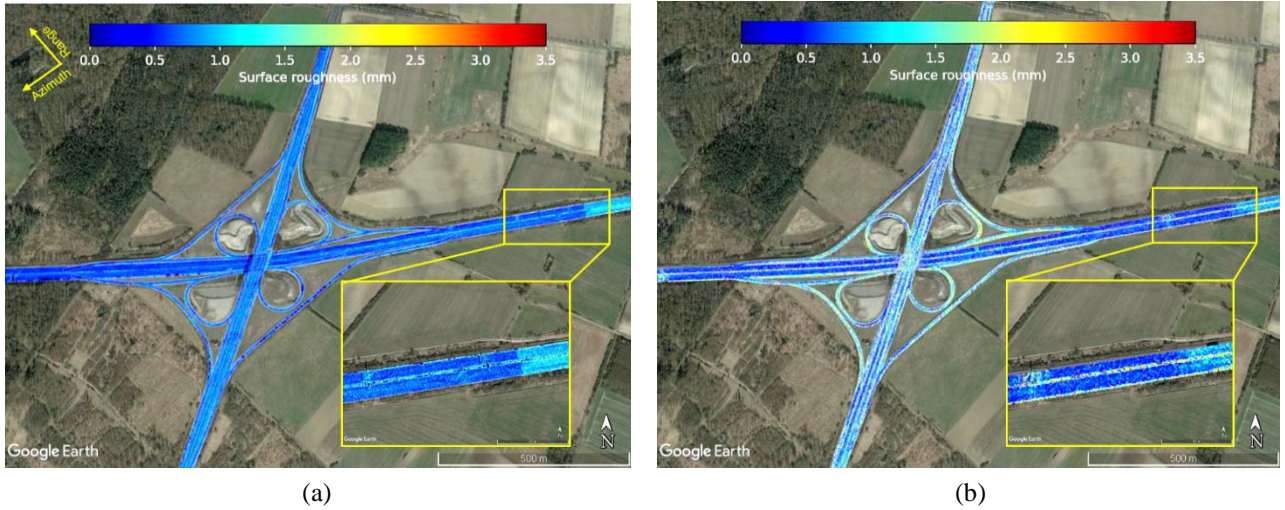


**Figure 8**  $h_{\text{rms}}$  images for the Braunschweig study area. (a) From a single F-SAR dataset. (b) Fused  $h_{\text{rms}}$  image from two TS-X datasets using multi-dataset averaging data fusion method.

## 5 Conclusion

This study presents an innovative approach for assessing road surface roughness utilizing high-resolution spaceborne SAR datasets. The staring spotlight TS-X datasets used in this study demonstrated notable sensitivity to surface variations, highlighting their potential for large-scale road surface roughness ( $h_{\text{rms}}$ ) estimation. The  $h_{\text{rms}}$  results obtained using the adapted semi-empirical model exhibited good agreement with both the F-SAR results and GT data. Nevertheless, the low SNR of the TS-X data, especially for the HH-polarized datasets, poses a serious challenge for road roughness estimation. The most suitable TS-X datasets for road surface roughness estimation are the VV-polarized TS-X datasets acquired in ST mode with incidence angles in the range of 30 to 35 degrees. This choice is based on the fact that the highest possible spatial resolution can be achieved through the use of the ST-mode and a steeper incidence angle and VV polarization ensure higher SNR, both of which are essential for reliable  $h_{\text{rms}}$  estimation. Post-processing of the  $h_{\text{rms}}$  images by applying the upper  $\sigma^0$  and lower SNR thresholds are essential to eliminate invalid  $h_{\text{rms}}$  values. In addition, the fusion of  $h_{\text{rms}}$  images generated from multiple datasets with different incidence angles and acquisition geometries can be performed using the multi-dataset averaging technique to improve the quality of the results. Road extraction and Google Earth visualization approaches can help in the interpretation of the results. Looking ahead, the use of future high-resolution wide-swath SAR systems (HRWS) with bandwidths up to 1200 MHz and improved noise-equivalent sigma zero (NESZ) can significantly improve the accuracy of road surface roughness estimates. In addition, using SAR technology to regularly monitor road conditions can identify potential problems early and facilitate predictive maintenance. This predictive approach can significantly extend the life of road networks, reduce maintenance costs, and improve overall road safety and efficiency.

## References

- [1] R. Ghandour, A. Victorino, M. Doumiati, and A. Charara, "Tire/road friction coefficient estimation applied to road safety," in *18th Mediterranean Conference on Control and Automation, MED'10*, 2010, pp. 1485–1490.
- [2] H. Liu, Z. Zhang, D. Guo, L. Peng, Z. Bao, and W. Han, "Research progress on characteristic technique of pavement micro-texture and testing technology of pavement skid resistance at home and abroad," in *2011 International Conference on Remote Sensing, Environment and Transportation Engineering*, 2011, pp. 4368–4372.
- [3] A. Babu, S. V. Baumgartner, and G. Krieger, "Approaches for Road Surface Roughness Estimation Using Airborne Polarimetric SAR," *IEEE JSTARS*, vol. 15, pp. 3444–3462, 2022.
- [4] E. Parliament *et al.*, *EU road surfaces : economic and safety impact of the lack of regular road maintenance*. Publications Office, 2014.
- [5] L. G. Rischioni, A. Babu, S. V Baumgartner, and G. Krieger, "Machine Learning Approaches for Road Condition Monitoring Using Synthetic Aperture Radar," *IEEE JSTARS*, 2023.
- [6] A. Babu, D. Gerber, S. V Baumgartner, and G. Krieger, "Road Surface Roughness Estimation Using Spaceborne Synthetic Aperture Radar," *IEEE GRSL*, p. 1, 2023.
- [7] I. Hajnsek, "Inversion of Surface Parameters Using Polarimetric SAR," Friedrich Schiller University Jena, 2001.
- [8] Airbus Defence and Space, "TerraSAR-X Image Product Guide," Mar. 2015.
- [9] Airbus Defence and Space, "Radiometric Calibration of TerraSAR-X Data," Mar. 2014.
- [10] P. C. Dubois, J. van Zyl, and T. Engman, "Measuring soil moisture with imaging radars," *IEEE TGRS*, vol. 33, no. 4, pp. 915–926, Jul. 1995.